metals

MDPI

Article

A Mineralogical Assessment on Residues after Acidic Leaching of Bauxite Residue (Red Mud) for Titanium Recovery

Gözde Alkan [1,*], Claudia Schier [1], Lars Gronen [2], Srecko Stopic [1] and Bernd Friedrich [1]

[1] IME-Process Metallurgy and Metal Recycling, RWTH Aachen University, Intzestraße 3, 52056 Aachen, Germany; cschier@ime-aachen.de (C.S.); sstopic@ime-aachen.de (S.S.); bfriedrich@ime-aachen.de (B.F.)

[2] IML-Chair of Applied Mineralogy and Economic Geology, RWTH Aachen University, Wüllnerstraße 2, 52062 Aachen, Germany; gronen@emr.rwth-aachen.de

* Correspondence: galkan@ime-aachen.de; Tel.: +49-24195873

Received: 27 September 2017; Accepted: 23 October 2017; Published: 28 October 2017

Abstract: Due to its alkalinity, red mud produced by the Bayer process may affect both the environment and human health. For this reason, its further utilization instead of disposal is of great importance. Numerous methods have already been studied for hydrometallurgical treatment of red mud, especially for the recovery of various metallic components such as iron, aluminum, titanium or rare earth elements. This study focuses on the extraction of titanium from red mud and in particular the mineralogical changes, induced by leaching. Sulfuric acid, hydrochloric acid and their combination have been utilized as leaching agents with the same leaching parameters. It has been determined that sulfuric acid is the best candidate for the red mud treatment in terms of titanium leaching efficiency at the end of 2 h with a value of 67.3%. Moreover, samples from intermediate times of reaction revealed that leaching of Ti exhibit various reaction rates at different times of reaction depending on acid type. In order to explain differences, X-ray Diffraction (XRD), scanning electron microscope (SEM) and QEMSCAN techniques were utilized. Beside titanium oxide (TiO_2) with available free surface area, a certain amount of the TiO_2 was detected as entrapped in Fe dominating oxide. These associations between Ti and Fe phases were used to explain different leaching reaction rates and a reaction mechanism was proposed to open a process window.

Keywords: bauxite residue; red mud; leaching; titanium; metal recovery

1. Introduction

There are growing efforts in industry to promote the sustainability and implementation of zero-waste production; the use of waste products from industrial processes is becoming increasingly important. During alumina production by Bayer process, a large amount of bauxite residue (red mud) is formed as a waste product [1–3]. The cumulative amount of red mud by 2015 is estimated to be close to 4×10^9 tons. These higher production rates and precious mineral content such as Fe_2O_3, Al_2O_3, SiO_2, TiO_2, Na_2O and CaO and rare earth elements induced the utilization of red mud as a secondary resource [4,5]. Reduced process costs with respect to primary metal production routes favors red mud usage in economic aspects. Moreover, valorization of such a highly alkaline product stored in the environment also provides ecological benefits [4]. Red mud can also be considered a secondary source of the most important modification of titanium compound, titanium dioxide. Owing to its outstanding properties, in particular its high refractive index, titanium dioxide is commonly used as white pigment in numerous fields of industry such as, dyes, plastics or even eatables and drugs [6,7]. Due to decreasing availabilities as well as qualities of the titanium ores, recovery of titanium from

red mud by hydrometallurgical methods gains importance. Depending on the source, red mud may exhibit higher amount of Ti (up to 25%), which affects leaching efficiency and selectivity [6]. There have been many studies conducted on titanium recovery from red mud by hydrometallurgical methods [6]. Among other inorganic acids, sulfuric acid (H_2SO_4) is reported as the best choice for higher titanium leaching efficiencies followed by chloric acid (HCl) [4]. Ti extraction rates reached 71% in the case of sulfuric acid leaching [7].

However, there is not a systematic study to explain the differences in leaching mechanisms and kinetics depending on acid type. This lack of knowledge leads to the detailed phase and mineralogical investigation on red mud and leach residue to open a process window. Hydrochloric acid, sulfuric acid and their combination were utilized as leachate with identical leaching conditions. Differences and similarities in leaching efficiencies and kinetics revealed by inductively plasma optical emission spectometryanalysis were explained using X-ray Diffraction (XRD), scanning electron microscope (SEM) and QEMSCAN techniques. A new leaching model was proposed for HCl and H_2SO_4 and difficulties of titanium dissolution from red mud were explained in detail.

2. Materials and Methods

2.1. Chemical Composition of Red Mud

The red mud used for this study was generated in Aluminum of Greece (Boeotia, Greece) S.A. The chemical composition of the red mud is listed in Table 1 and shows the major constituents of this material such as iron (III)-oxide, aluminum oxide, calcium oxide and silicon dioxide analyzed by inductively plasma Optical Emission Spectrometry.

Table 1. Chemical composition of red mud.

Composition	wt %
Fe_2O_3	42.34
Al_2O_3	16.26
Ignition loss	12.66
CaO	11.64
SiO_2	6.97
TiO_2	4.27
Na_2O	3.83
Others	1.85
La_2O_3	0.09
CeO_2	0.06
Sc_2O_3	0.02
Nd_2O_3	0.01
Y_2O_3	0.01

2.2. Experimental Method

A typical leaching test was performed with a heating plate and magnetic stirrer to control the temperature and stirring speed. The leaching efficiencies of sulfuric acid, hydrochloric acid and a combination of the two acids in the ratio of hydrochloric acid to sulfuric acid of 1:3 were investigated with the same leaching parameters. The experiments were carried out at a set temperature of 70 °C, 360 rpm and a 4-molar acid concentration. The solid-liquid ratio was adjusted to a ratio of 1:50 in order to prevent silica gel formation. In order to reveal leaching rates as a function of reaction time, for all three acids, leaching duration was varied as 5, 15, 30, 60, 90 and 120 min. At the end of reaction time, samples were vacuum filtrated for solid and liquid separation. Solid residues were dried overnight at 90 °C and prepared for characterization. For XRD analyses, dried particles were milled to prevent scattering effect. However, they were analyzed as dried version by SEM and QEMSCAN so as not to retain available free surface areas of minerals. Leach liquor was diluted 20 times for ICP analyses.

2.3. Materials Characterization

Automated quantitative mineralogy analyses of red mud and solid residues were performed using a Qanta-650 F (FEI corporate headquarters, North America Nanoport, Hillsboro, OR, USA) QEMSCAN scanning electron microscope (SEM). The particular samples were embedded into epoxy resin to form blocks of approx. 25.4 mm in diameter. For analysis by SEM, the sample surface was polished and carbon coated to give best analytical results and to avoid surface charging during electron bombardment [8]. The system mounts 2 DualX-Flash (Bruker AXS, Karlsruhe, Germany) energy-disperse detectors for recording X-ray spectra emitted by the interaction of the electron beam with the atoms of the sample surface. Additionally, a 4 quadrant backscatter electron and a secondary electron (SE) detector are installed for image acquisition.

For QEMSCAN analysis, the acceleration voltage was set to 25 kV. The sample current was set to 10 nA at a working distance of 13 mm. The point spacing was set to 7.5 μm per step and 2000 X-ray counts were recorded per step. Phase interpretation and further image analysis, like phase map, modal composition and elemental mapping, were performed by using iDiscover software suite (FEI).

Back scattered electron (BSE) and secondary electron (SE) image acquisition were performed by the same system in SEM-mode using an acceleration voltage of 15 kV. For a better resolution of the images the working distance was decreased to 11.7 μm.

XRD analyses was performed by Bruker D8 Advanced Diffractometer (Bruker AXS, Karlsruhe, Germany), which use Bragg-Brentano Geometry and θ–θ synchronization for X-Ray tube and the detector. 10°–80° (2θ) were scanned with a 5°/min rate. The generator voltage was 40 kV and current was 40 nA. The quantitative evaluation was carried out with the program Topas (Bruker, AXS, Karlsruhe, Germany). For Rietveld analysis, the full profile method was used; 0-point errors, specimen height errors, diffraction-peak intensities, Lorantz Polarisation (LP)-factor, background and crystal structure models were refined.

3. Results and Discussion

The evaluation of titanium leaching efficiencies as a function of reaction time can be seen in Figure 1. The graph represents the average leaching values, including deviations due to test repetitions. At the end of two hours, the highest leaching efficiency of titanium (67.3%) was achieved with sulfuric acid, followed by hydrochloric acid (59.8%) and the combination of HCl to H_2SO_4 with a ratio of 1:3 (56.4%).

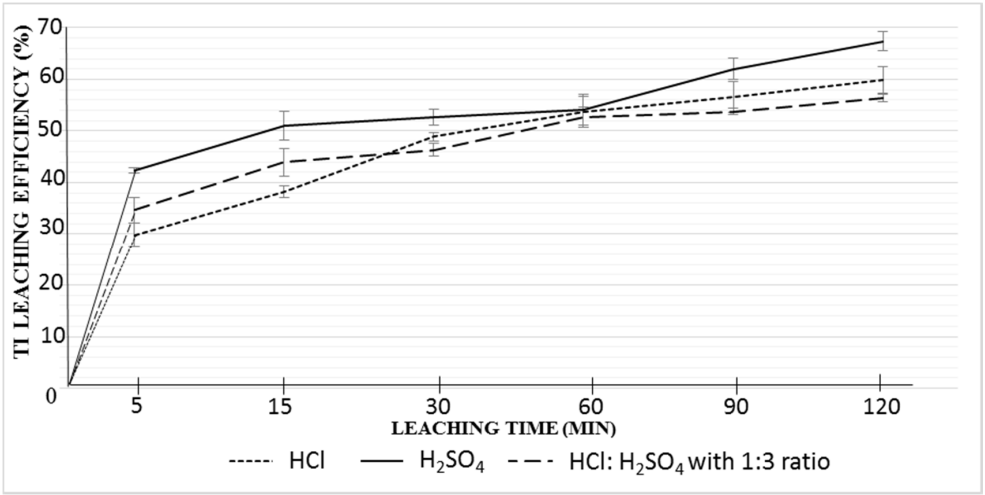

Figure 1. Leaching efficiencies of Ti with various acids (where 100% Ti efficiency corresponds to 0.94 g Ti in 1 L acid solution).

Moreover, the time dependent evaluation of leaching efficiencies revealed variable kinetic profiles after three different acid treatments. In the first 15 min of leaching, for all acid types, higher leaching rates were observed by a higher slope of the curves. After 15 min, in the case of H_2SO_4, the leaching rate decreases until 60 min test duration. In contrast, during this period (15–60 min), there is still high leaching rates observed with hydrochloric acid. After 60 min, it is seen that the HCl leaching curve gets closer to saturation and leaching becomes slower, while H_2SO_4 reaches higher rates and superior leaching efficiency. The course of the combination of hydrochloric- and sulfuric acid is characterized by less significant leaps. From this data it is seen that the most efficient leachate in terms of final leaching efficiency for Ti is sulfuric acid. However, the findings on leaching kinetics induced the detailed investigation of leaching to explain different mechanisms by different leachates and find an optimum process condition.

Using X-ray diffraction, the phase content of solid residues after HCl and H_2SO_4 treatment were investigated to reveal the effect of acid type on leaching mechanism. Related XRD analyses are given in Figure 2a,b for direct comparison purposes.

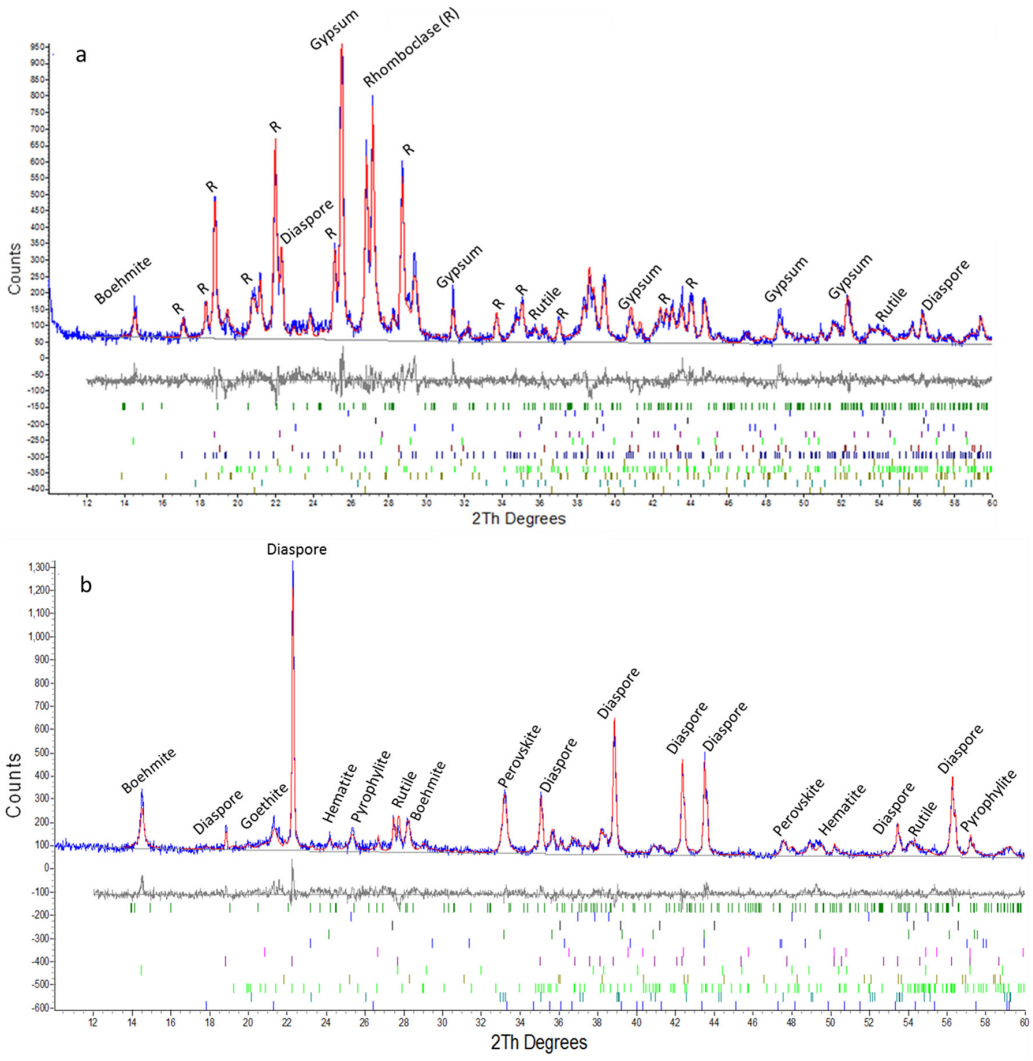

Figure 2. X-ray Diffraction (XRD) analyses of solid residues at the end of 2 h: (**a**) H_2SO_4 and (**b**) HCl leaching with Rietveld refinement (blue line is experimental, red line is calculated and the difference below with marked reflection positions).

Table 2. Quantitative analyses of sulfuric acid (H_2SO_4) and chloric acid (HCl) residues.

Composition	H_2SO_4 Residue (%)	HCl Residue (%)
Rutile (TiO_2)	0.58	1.50
Anatase (TiO_2)	0.81	0
Perovskite ($CATiO_3$)	0	3
Hematite (Fe_2O_3)	0	5.3
Goethite (FeO(OH))	0.167	6.3
Rhomboclase ($HFe(SO_4)_2 \cdot 4(H_2O)$)	57.4	0
$FeSO_4 \cdot 6H_2O$ *	3.47	0
Diaspore (AlO(OH))	15.39	60
Boehmite (AlO(OH))	2.75	10
Pyrophylite ($Al_2[(OH)_2] \mid Si_4O_{10}$)	1.8	9.4
Quartz (SiO_2)	0	0.1
Crotobalite (SiO_2)	0.61	0.193
Gypsum ($CaSO_4 \cdot 2H_2O$)	12.45	0
Albite ($Na(AlSi_3O_8)$)	2.4	3.06

* unnamed, possibly an Fe-analogue of retgersite.

XRD analyses revealed the differences in phase contents of leach residues in terms of titanium (Ti), iron (Fe) including phases, which may explain the different leaching behavior of two acids. As listed in Table 2, total amount of Fe including phases (hematite (5.3%) and goethite (6.3%)) are low in HCl solid residue. Nevertheless, it is seen that H_2SO_4 residue is much more enriched in terms of Fe compounds such as, rhomboclase, another iron sulfate and trace amounts of goethite. A higher amounts of Fe is found as rhomboclase (57.4%) which is formed by re-precipitation of dissolved Fe ions with sulfate. In the presence of sulfate ions and highly acidic conditions provided by concentrated H_2SO_4 leachate, the precipitation of dissolved Fe into rhomboclase is thermodynamically more favorable and may result in less leaching efficiency of Fe [9]. Quantitative analyses of residues imply in parallel with ICP analyses, higher Fe dissolution rates in the presence of HCl. Moreover, at the end of 2 h HCl leaching, Ti was detected in HCl leach residue in the form of perovskite (3%) and rutile (1.5%). In contrast, Ti was found only as rutile (0.58%) and anatase (0.81%) in the H_2SO_4 leach residue with relatively lower amounts (see Table 2), implying higher leaching efficiencies in parallel with ICP findings. Perovskite may be consumed by the reaction of calcium with sulfate ions and precipitate into gypsum as revealed in X-ray diffractogram of H_2SO_4 slag; which may also favor Ti extraction from perovskite. Higher Ti and lower Fe leaching efficiencies with H_2SO_4 favor its utilization for selective Ti leaching from red mud.

Nonetheless, when 4 wt % content of Ti in red mud and even lower value for residue is considered, XRD is not highly sensitive to reveal changes in Ti including phases. This lack of sensitivity induced QEMSCAN utilization which can deal with elemental and phase mappings, phase associations and available surface area detections for red mud and the most promising leachate (H_2SO_4) residue.

In Figure 3, the Ti elemental mapping of red mud and leach residue are given together for direct comparison purposes. The field scan image of red mud in Figure 3 revealed that Ti content of red mud phases is inhomogeneous with a maximum amount of 8–9 wt %. After leaching, a dramatic change in distribution is observed, which exhibits homogenous and finely distributed Ti through the minerals of H_2SO_4 residue with a decreased amount at a maximum 3–4 wt %.

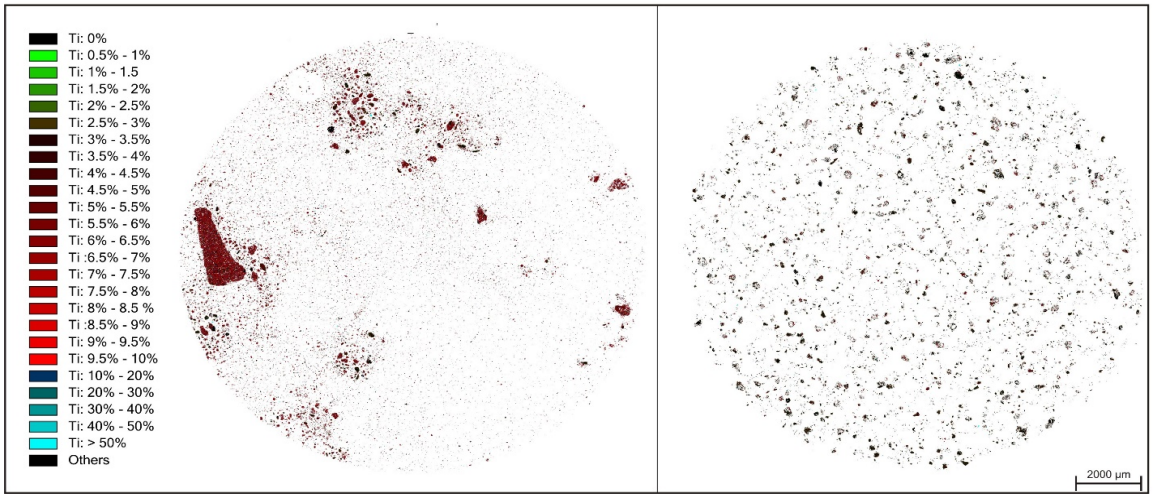

Figure 3. Ti elemental mapping of red mud (left) and H_2SO_4 leach residue (right) by QEMSCAN analyses.

Beyond elemental mapping, the mineral distribution within red mud and H_2SO_4 leach residue were also investigated in a comparative manner.

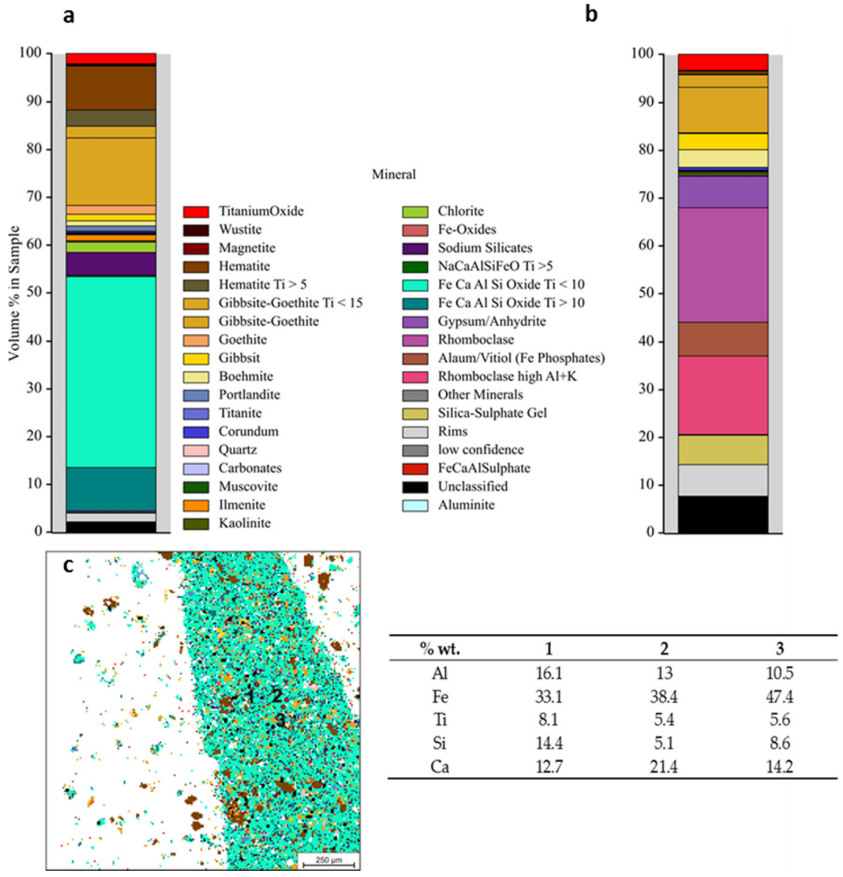

% wt.	1	2	3
Al	16.1	13	10.5
Fe	33.1	38.4	47.4
Ti	8.1	5.4	5.6
Si	14.4	5.1	8.6
Ca	12.7	21.4	14.2

Figure 4. Mineral distribution of red mud: (**a**) and H_2SO_4 leach residue (**b**) with detailed compositional analyses (**c**) reveled by QEMSCAN and table represents chemical compositions of points labeled as 1, 2 and 3.

In addition to phases indicated by XRD, QEMSCAN, analysis given in Figure 4 revealed the presence of large amounts of Fe-, Ca-, Al-, Si mixed oxide in red mud, where a certain amount of TiO_2 is entrapped. Due to the heterogeneous nature of this complex oxide, chemical composition and stoichiometry vary through the volume. Therefore, a crystalline phase could not be assigned. Varying compositions revealed by point 1, 2 and 3 imply that this complex oxide may be aggregate or intergrowth of several oxides inherent from Bayer Process. After leaching with H_2SO_4, as represented in the mineral distribution in Figure 4b, it is seen that most of this various composed oxide is leached out and rhomboclase formation takes place as consistent with XRD analysis. In leach residue, a limited amount of TiO_2 is detected only within gibbsite-goethite as revealed in Figure 4b.

The mineral association analysis revealing free available surfaces and contacts between phases is represented in Figure 5a,b for red mud and H_2SO_4 leach residue respectively.

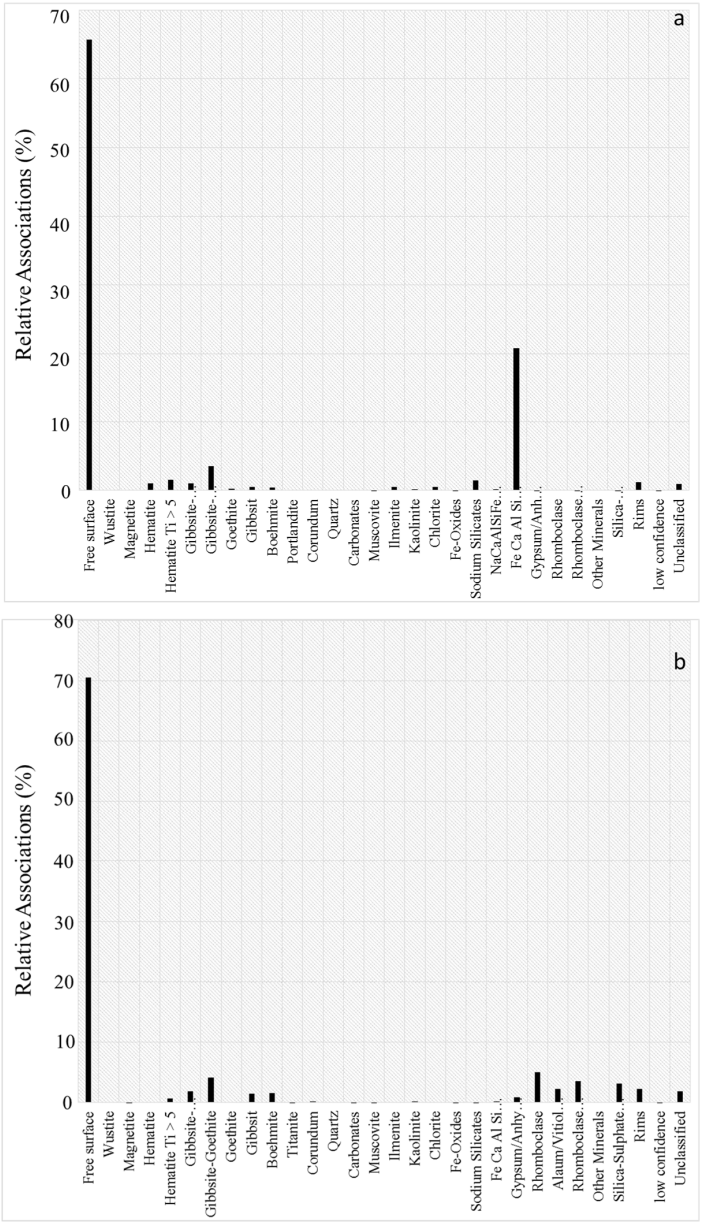

Figure 5. Mineral association of TiO_2 within: (**a**) red mud; (**b**) H_2SO_4 leach residue.

Figure 5a exhibits that certain amounts of TiO_2 surfaces are in contact with Fe-, Ca-, Al-, Si-oxide. The remaining TiO_2 was found with free available surfaces, which may result in fast leaching kinetics in the very early stage of leaching revealed by ICP analyses given in Figure 1. In comparison with red mud, when H_2SO_4 leach residue is considered as represented in Figure 5b, it is seen that most of the TiO_2 surfaces are free and available, just very negligible quantities are in contact with rhomboclase and gibbsite-goethite. These findings reveal that the Fe dominating complex composed oxides form a diffusion barrier between TiO_2 and leachate and may be the reason for the deceleration of reaction kinetics in the middle period of the trial.

Red mud and H_2SO_4 leach residue were investigated in a comparative manner by SEM to reveal morphological changes taking place during leaching, as represented in Figure 6. In order to reveal elemental composition, Energy dispersive X-Ray analyses (EDX) was also utilized.

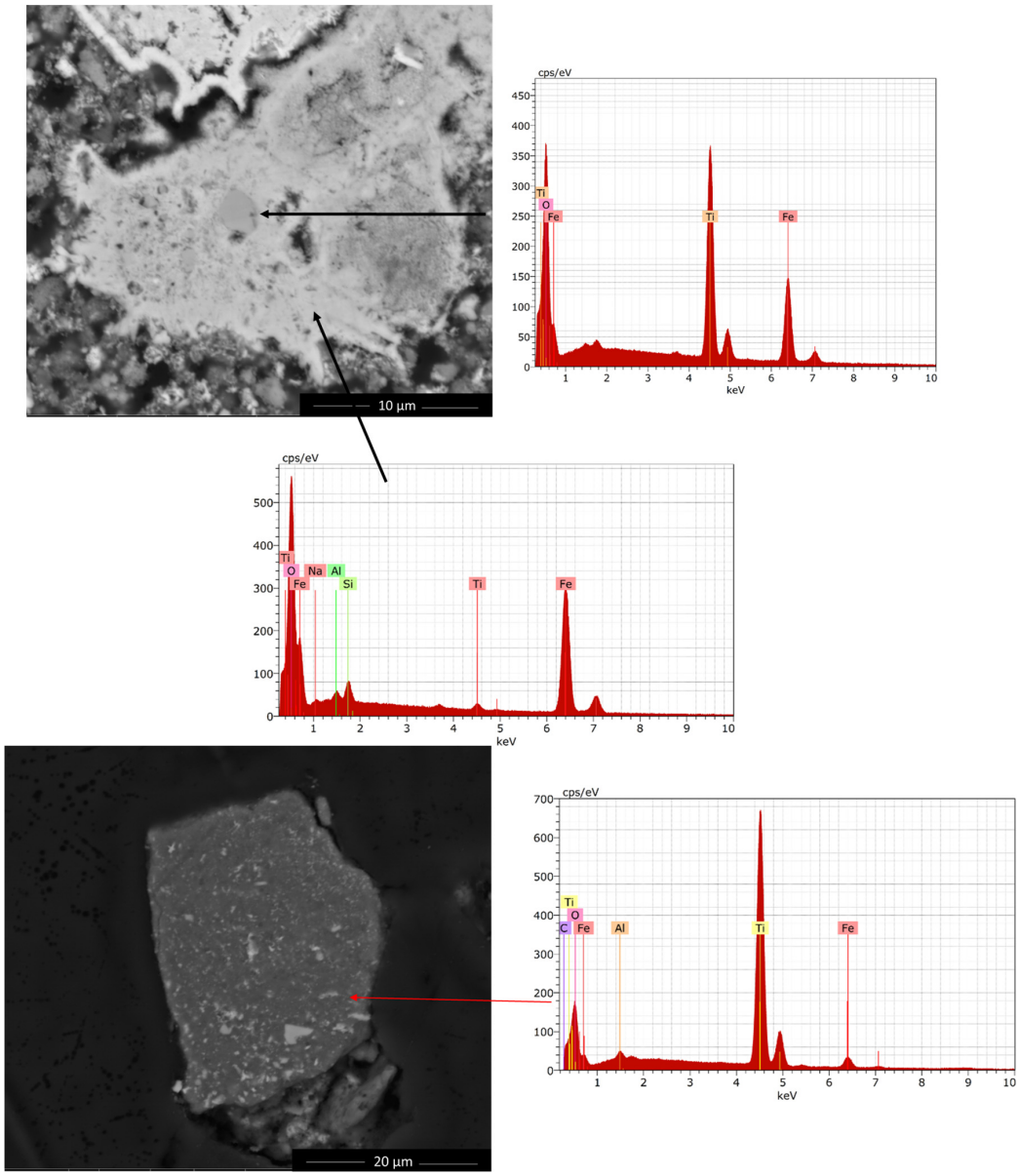

Figure 6. Scanning electron microscope (SEM) micrographs of red mud (above) and H_2SO_4 leach residue (below).

Relatively large aggregates around 30 μm of Fe (also Al, Si and Na including) dominating oxides have been revealed where 2–3 μm sized TiO_2 is entrapped in parallel with findings of QEMSCAN. This micrograph emphasizes that in order to reach to TiO_2 enriched compound, the more iron oxide enriched phase should be leached out. On the other hand, leach residue exhibited relatively finer particles with respect to coarser aggregates of red mud. Moreover, in leach residue, mostly TiO_2 is detected with free surfaces and small contact with Al dominating oxide where some Fe is also present, as represented in Figure 6. This is consistent with QEMSCAN analyses which indicates mostly free surfaces of TiO_2 and a trace amount of contact with gibbsite-goethite.

Presence of both free and entrapped TiO_2 surfaces revealed by SEM and QEMSCAN may be responsible for various leaching kinetic regimes within various stages of reaction. Since leaching starts from surface, initial high leaching kinetic for all acid treatments is owing to easy access to TiO_2 surfaces. The second regime, as observed in Figure 1, starts from 15 min of reaction where H_2SO_4 has slower and HCl similar behavior with respect to the first regime. It is worth emphasizing that as reported in previous studies, H_2SO_4 is more sensitive to TiO_2 leaching where HCl was used to dissolve Fe [10]. Their selectivity to metal types may be the reason for different kinetics in the second regime. Faster Fe leaching in the earlier stages of reaction by HCl ensures leachate to access TiO_2 entrapped in Fe dominating oxide. Relatively lower leaching rates of Fe in the case of H_2SO_4 may result in highly pronounced diffusion barrier effect of Fe enriched oxide for leaching of TiO_2 However, after this time H_2SO_4 achieves higher kinetics, most probably due to increased Fe leaching with longer reaction times. In the end, H_2SO_4 yields in higher Ti leaching efficiency as consistent with previous studies [10,11].

Iron oxide enriched phase inhibiting effect implied by SEM and QEMSCAN is analyzed by ICP measurement to reveal Fe leaching rates with HCl and H_2SO_4. Figure 7a,b represent leaching rates of Fe and Ti for H_2SO_4 and HCl respectively.

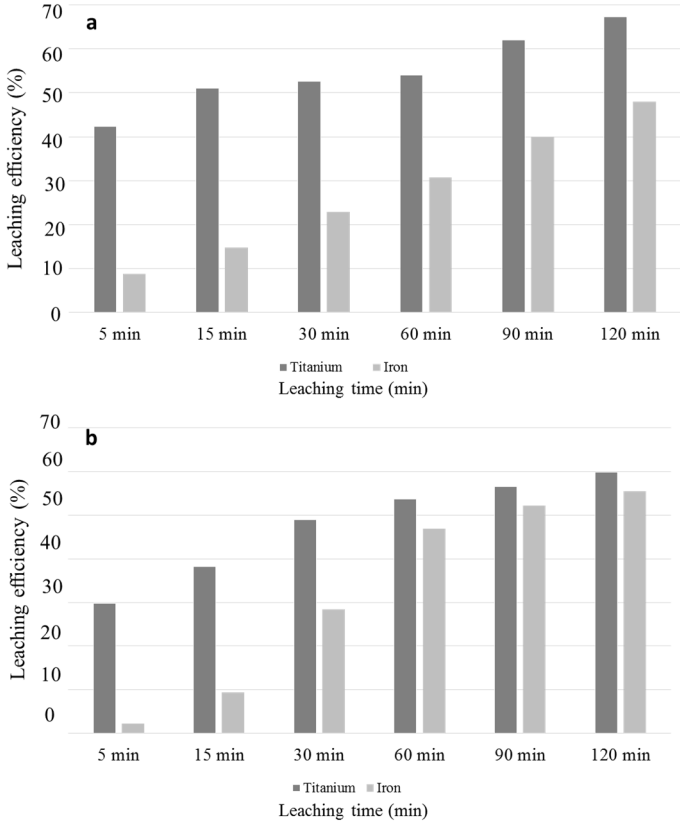

Figure 7. Titanium and iron leaching efficiencies by (**a**) sulfuric acid; (**b**) hydrochloric acid leaching (where 100% Ti and Fe leaching efficiencies corresponds to 0.94 g Ti and 8.47 g Fe in 1 L acid solution).

Figure 7a,b reveal that Fe leaching rates are similar in the early stages of leaching. However, after 15 min of reaction, Fe oxide dissolution is increased dramatically with HCl. Although they are quite similar in the early stages of reaction, after 15 min, an increase in HCl leach rate is observed while that in H_2SO_4 is still slow. After 60 min of reaction, only 30% of iron is leached out by H_2SO_4, while 46% by HCl. After 60 min, Fe leaching rate by H_2SO_4 becomes also higher and achieved to 47% at the end of 2 h, while HCl reached 55%. After 60 min, leaching rates of Ti by H_2SO_4 accelerates. Increasing Ti leaching rates with increasing Fe dissolution, in parallel with SEM and QEMSCAN analyses, indicate the obstacle effect of Fe oxide enriched mineral over Ti recovery. More leached out Fe enriched oxide favors the access of leachate to the entrapped TiO_2, which results in higher kinetics of H_2SO_4 in the last stage of the leaching.

In light of SEM, QEMSCAN and ICP analyses, a model for leaching process with HCl and H_2SO_4 are proposed as in Figure 8. This model is based on already existing particle dissolution model in leaching, where the reaction starts from surface and propogates through the core.

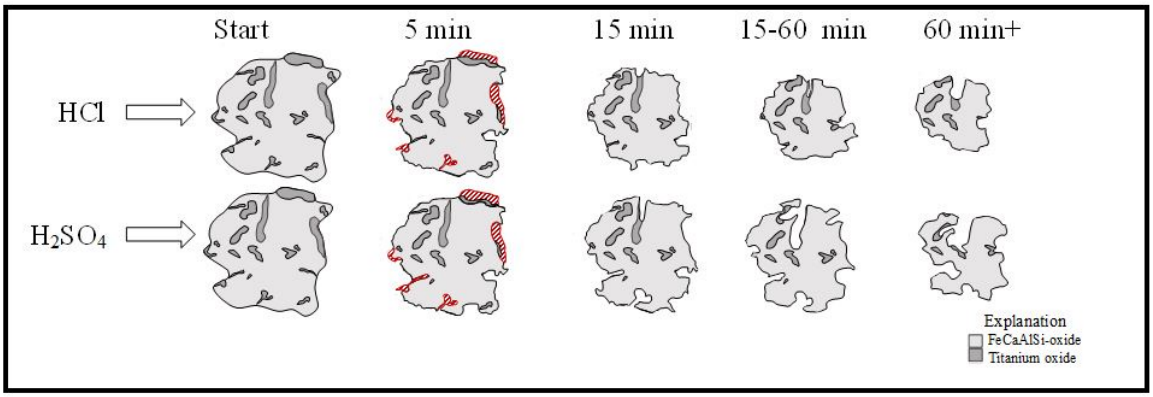

Figure 8. Dissolution model of particles by hydrochloric acid and sulfuric acid leaching.

After a period of 5 min, more TiO_2 is dissolved in sulfuric acid compared with hydrochloric acid. This can be seen in the red hatching in Figure 8. Due to the higher sensitivity of hydrochloric acid leaching to iron, in the middle time of leaching after free TiO_2 surfaces are consumed, HCl achieves entrapped TiO_2 more easily and exhibits faster kinetics. However, after 60 min, H_2SO_4 also leaches a certain amount of Fe for the exposure of TiO_2 from the Fe Ca Al Si-oxide. The remaining TiO_2 particles are leached out after a time of 60 min and at the end of reaction less amount of TiO_2 remains in residue of H_2SO_4 with respect to that of HCl.

4. Conclusions

A detailed examination of the red mud leaching was carried out to reveal mineralogical changes with various acid types in order to explain the dissolution of titanium from red mud. At the end of two hours of leaching, the highest sensitivity to titanium dissolution is observed with a value of 67% in the case of sulfuric acid leaching. Moreover, Ti and Fe leaching rates as a function of reaction time have been investigated. A mineral association between Ti and Fe and the importance of available surfaces of titanium including particles on leaching efficiency were reported. It was pointed out that Fe has an obstacle effect on Ti leaching and there should be a certain amount of Fe dissolution for better Ti leaching.

Acknowledgments: The authors wish to thank the Aachen Know-How Centre Resource Technology (AKR) for the support of an open access. This research is founded by European Community's Horizon 2020 Programme ([H2020-MSCA-ITN-2014]) under Grant Agreement No. 636876 (MSCA-ETN REDMUD). Authors also acknowledge Yiannis Pontikes, Koen Binnemans, Ken Evans and George Blagovyi for their valuable support.

Author Contributions: Claudia Schier and Gözde Alkan designed and performed the experiments; Gözde Alkan, Claudia Schier, Bernd Friedrich analyzed the data; Srecko Stopic and Lars Gronen contributed reagents/materials/analysis tools; Gözde Alkanand, Claudia Schier wrote the paper.

Conflicts of Interest: The authors declare no conflicts of interest.

References

1. Klauber, C.; Gräfe, M.; Power, G. Bauxite residue issues: II. Options for residue utilization. *Hydrometallurgy* **2011**, *108*, 11–32. [CrossRef]
2. Piga, L.; Pochetti, F.; Stoppa, L. Recovering metals from red mud generated during alumina production. *J. Miner. Met. Mater. Soc.* **1993**, *45*, 54–59. [CrossRef]
3. Zhang, W.; Zhu, Z.; Cheng, C.Y. A literature review of titanium metallurgical processes. *Hydrometallurgy* **2011**, *108*, 177–188. [CrossRef]
4. Lim, K.; Shon, B. Metal Components (Fe, Al and Ti) recovery from red mud by sulfuric acid leaching assisted with ultrasonic waves. *Int. J. Emerg. Technol. Adv. Eng.* **2015**, *5*, 25–32.
5. Agatzini-Leonardou, S.; Oustadakis, P. Titanium leaching from red mud by diluted sulfuric acid at atmospheric pressure. *J. Hazard. Mater.* **2008**, *157*, 579–586. [CrossRef] [PubMed]
6. Kasliwal, P.; Sai, P.S.T. Enrichment of titanium dioxide in red mud: kinetic study. *Hydrometallurgy* **1999**, *53*, 73–87. [CrossRef]
7. Ghorbani, A.; Fakhariyan, A. Recovery of Al_2O_3, Fe_2O_3 and TiO_2 from bauxite processing waste (red mud) by using combination of different acid. *J. Basic. Appl. Sci. Res.* **2013**, *3*, 187–191.
8. Reed, S.J.B. *Electron Microprobe Analysis and Scanning Electron Microscopy in Geology*; Cambridge University Press: Cambridge, UK, 2005.
9. Gil, A.; Salgado, L.; Galicia, L.; Gonzales, I. Predominance-zone diagrams of Fe(III) and Fe(II) sulfate complexes in acidic media. *Talanta* **1995**, *42*, 407–414. [CrossRef]
10. Borra, C.R.; Pontikes, Y.; Binnemans, K.T.; Gerven, V. Leaching of rare earths from bauxite residue (red mud). *Miner. Eng.* **2015**, *76*, 20–27. [CrossRef]
11. Sayan, E.; Bayramoglu, M. Statistical modeling of sulfuric acid leaching of TiO_2 from red mud. *Hydrometallurgy* **2004**, *71*, 397–401. [CrossRef]